

Connections between deep tropical clouds and the Earth's ionosphere

M. E. Hagan,¹ A. Maute,¹ R. G. Roble,¹ A. D. Richmond,¹ T. J. Immel,²
and S. L. England²

Received 25 March 2007; revised 14 June 2007; accepted 13 September 2007; published 25 October 2007.

[1] We report on a series of simulations with the National Center for Atmospheric Research (NCAR) thermosphere-ionosphere-mesosphere-electrodynamics general circulation model (TIME-GCM) which were designed to replicate and facilitate the interpretation of the longitudinal structure discovered in IMAGE satellite airglow observations of the equatorial ionization anomaly (EIA) at the far-ultraviolet (FUV) 135.6-nm wavelength during March–April 2002 equinox. Our TIME-GCM results indicate that the four-peaked longitudinal variation in the EIA observed by IMAGE-FUV near 20:00 local solar time can be explained by the effects of an eastward propagating zonal wavenumber-3 diurnal tide (DE3) that is excited by latent heat release associated with raindrop formation in the tropical troposphere. **Citation:** Hagan, M. E., A. Maute, R. G. Roble, A. D. Richmond, T. J. Immel, and S. L. England (2007), Connections between deep tropical clouds and the Earth's ionosphere, *Geophys. Res. Lett.*, *34*, L20109, doi:10.1029/2007GL030142.

1. Introduction

[2] The equatorial ionization anomaly (EIA) is a fascinating feature of the low latitude ionosphere with daytime and evening electron-density maxima both north and south of the magnetic equator even during times when the ionospheric production peak is equatorial. The EIA is produced by the equatorial fountain, driven by the combined effects of the magnetic and electric fields in the near-Earth environment, but it is also intimately connected to the motion of the neutral atmosphere in the lower thermosphere. During the daytime, neutral winds at lower thermospheric heights (ca. 110–150 km) interact with the ionospheric plasma in the so-called E-region, causing the comparatively massive ions to be dragged along by the neutral particles, separating them from the electrons whose motion is constrained by the magnetic field. This process sets up an eastward electric field across the dayside of the atmosphere that extends upward into the F-region ionosphere and causes the plasma to drift upward. Diffusion by plasma pressure gradients and gravity subsequently effects the plasma motion, causing it to sink along the magnetic field and settle in locations north and south of the equator [e.g., *Appleton*, 1946]. Any variations in lower thermospheric daytime winds, such as

those associated with atmospheric tides will affect the equatorial fountain [e.g., *Fesen et al.*, 2000].

[3] Recent analyses of IMAGE FUV observations reveal four longitudinal EIA enhancements in the early evening, which can be attributed to comparatively stronger equatorial plasma fountain effects at each of these locations [*Sagawa et al.*, 2005; *Immel et al.*, 2006; *England et al.*, 2006a, 2006b]. These results complement related upper atmospheric diagnostics that also reveal longitudinal variability with 4 peaks [*Vladimer et al.*, 1999; *Jadhav et al.*, 2002; *Lühr et al.*, 2004; *Lin et al.*, 2007]. *Jadhav et al.* [2002] and *Sagawa et al.* [2005] suggested a connection to tidal effects, but *Immel et al.* [2006] were the first to assert that longitudinal variations in nonmigrating (i.e., not Sun-synchronous) tides of tropospheric origin could propagate upward into the lower thermosphere, affect the E-region dynamo process, and produce the 4-peaked patterns observed by IMAGE-FUV. To strengthen their claim they correlated their EIA enhancements with the 115-km diurnal tidal temperature variations predicted by the global-scale wave model (GSWM) [*Hagan and Forbes*, 2002]. Relatedly, *England et al.* [2006a] showed that daytime E-fields near 108 km are also well correlated with GSWM tidal variations.

[4] Herein, we report on first-principles calculations with the NCAR thermosphere-ionosphere-mesosphere-electrodynamics general circulation model (TIME-GCM), which replicate the IMAGE results and confirm that tides excited in the lower atmosphere can affect the EIA, and impact the ionosphere aloft. Finally, we identify the nonmigrating tidal component that is primarily responsible for the observed 4-peaked EIA structure, namely the eastward propagating wavenumber-3 diurnal tide.

2. TIME-GCM Simulations

[5] The TIME-GCM is the latest in the series of three-dimensional time-dependent NCAR models that were developed to simulate the circulation, temperature, electrodynamics, and compositional structure of the upper atmosphere and ionosphere. The TIME-GCM is a global grid-point model that calculates neutral gas heating, dynamics, photoionization, electrodynamics, and the compositional structure of the middle and upper atmosphere and ionosphere from first principles for a given solar irradiance spectrum which varies with solar activity. Sub-grid-scale gravity waves are necessary for realistic simulations of the mesopause region and are parameterized with a modified *Lindzen* [1981] type scheme that is extended to include molecular damping effects in the lower thermosphere. We refer the reader to *Roble and Ridley* [1994], *Roble* [1995, 1996], and references therein for a more complete description of the TIME-GCM.

¹High Altitude Observatory, National Center for Atmospheric Research, Boulder, Colorado, USA.

²Space Sciences Laboratory, University of California, Berkeley, California, USA.

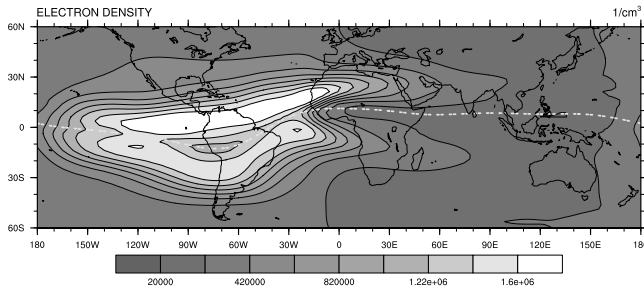


Figure 1. Contours of TIME-GCM log electron density (cm^{-3}) versus geographic longitude and latitude between 60°N and 60°S calculated with the standard IGRF at 20 UT and near 450 km. The dashed curve represents the location of the geomagnetic equator.

[6] For the simulations discussed herein, the TIME-GCM resolution was 2.5° by 2.5° in the horizontal and 4 grid points per scale height in the vertical. We invoked a 10.7-cm solar radio flux ($F_{10.7}$) value of 150, a hemispheric power value [after *Evans*, 1987] of 8 GW, and a cross-cap potential drop of 30 kV in our simulation of day of year 80 to represent solar radiative and auroral forcings during solar moderate and geomagnetically quiescent March conditions. These conditions are comparable to those that characterize the IMAGE-FUV data.

[7] The TIME-GCM inherently accounts for atmospheric tides that are excited by the absorption of ultraviolet and extreme ultraviolet radiation in the middle and upper atmosphere, but we need to account for tidal components of tropospheric origin that propagate upward into the model domain by perturbing the TIME-GCM lower boundary (i.e., 10 mb; ~ 30 km). We do this with the March horizontal wind, temperature, and geopotential height results from the global-scale wave model (GSWM), which account for tropospheric tides excited both by the absorption of infrared radiation and latent heat release associated with raindrop formation in deep convective clouds in the tropics [e.g., *Hagan and Forbes*, 2002, 2003]. These lower atmospheric waves are known to play an important role in the dynamics of the upper mesosphere and lower thermosphere [e.g., *Oberheide et al.*, 2006].

[8] Our TIME-GCM calculations are aimed at replicating and understanding the EIA longitude variability observed by IMAGE and exploring related impacts in the ionosphere-thermosphere system. In order to separate sources of variability that originate in the troposphere from sources associated with ionosphere-thermosphere processes excited in-situ, we devised 2 sets of simulations, employing 1) the standard magnetic field specified by the International Geomagnetic Reference Field (IGRF), and 2) a dipole geomagnetic field aligned with the Earth's axis. We refer to these runs as the IGRF and aligned dipole runs, respectively. The offset between the geographic equator and IGRF geomagnetic equator that varies with longitude is evident in Figure 1 (dashed line). The associated variations in the low latitude geomagnetic field points to inherent longitudinal variability in the processes that couple the ionosphere and

thermosphere. Differences between TIME-GCM IGRF and aligned dipole results, in the absence of TIME-GCM lower boundary perturbations, allow us to quantify longitudinal variability that is generated from first principles within the model domain and is primarily associated with the offset between the geographic and geomagnetic coordinate systems at upper atmospheric altitudes.

[9] We further quantify upper atmospheric variability by isolating the responses attributable to tropospheric tides by differencing the TIME-GCM results with and without GSWM tropospheric tidal excitation at the model lower boundary. We do this for both of the IGRF and aligned dipole field configurations. The IGRF results that include GSWM tidal forcing at the lower boundary constitute our realistic simulation, which we compare with the IMAGE data.

3. Results

[10] Figure 1 illustrates a synoptic map or snapshot of electron density results from the realistic TIME-GCM simulation (i.e., IGRF with tropospheric tidal forcing) at 20 UT near 450 km (i.e., pressure level 4). We exclude the results poleward of 60° in order to better focus on the signatures of the EIA, which are clearly evident in the dayside and evening ionosphere between about 150°W and 80°E longitude. The illustrated ionization peaks are symmetric (asymmetric) with respect to the geomagnetic (geographic) equator in the western hemisphere. The symmetry is particularly notable between about 50°W and 90°W where the geomagnetic equator is markedly south of the geographic equator. Notably, the simulated EIA extends into the dusk sector (30°W to 30°E), where IMAGE-FUV observed zonal wavenumber-4 variations in synoptic maps of the EIA near 20–22 local solar time (LST) [*Immel et al.*, 2006].

[11] The synoptic map of the difference between the TIME-GCM electron densities at 20 UT and ~ 450 km illustrated in Figure 1 and those calculated with the IGRF but without tropospheric tidal forcing is shown in Figure 2a. Pronounced correlative maxima near $150\text{--}160^\circ\text{W}$, 0° and 90°E are apparent at 10°N , but these features evolve significantly as a function of latitude in the tropics. These differences isolate the effects of the troposphere on the ionosphere, but they are also affected by ion-neutral coupling processes via the IGRF. Differences between the aligned dipole simulations with and without tropospheric tides (Figure 2b) eliminate these features, and exhibit correlative maxima at similar locations, which are far more symmetric across the tropical latitude region. Both figures provide evidence that a distorted zonal wavenumber-3 feature is modulating the expected day-night differences in the low-latitude F-region ionosphere. Notably, strong EIA enhancements associated with this feature are near 160°W and 0° (Figure 2).

[12] In order to compare our TIME-GCM electron density results with FUV brightness observed by IMAGE we have to examine the former from the satellite perspective. This requires an synoptic view of electron density as a function of longitude and latitude but at a constant local solar time, and here we select 20 LST. It is equally

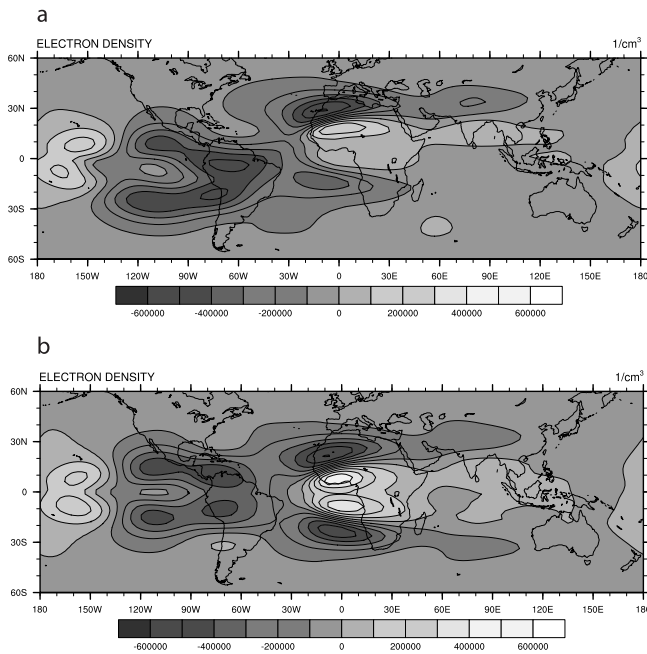


Figure 2. (a) Contours of electron density (cm^{-3}) differences from TIME-GCM simulations with/without tropospheric tides for the standard IGRF simulations versus longitude and latitude at 20 UT. (b) Same as Figure 2a, except for the aligned dipole geomagnetic field.

important to note that a zonal wavenumber-3 oscillation will appear as a 4-peaked structure in an asymptotic constant local time map. Figure 3 is an asymptotic diagnostic of the peak TIME-GCM electron density at 20 LST and between 250 and 500 km between the equator and 45°N as a function of longitude for our four simulations. As anticipated, the peak density from the aligned dipole simulation that excludes tidal forcing is longitude invariant. But, there is a 4-peaked structure in the aligned dipole simulation with tropospheric tides. This TIME-GCM EIA variability is solely attributable to the tropospheric source. The remaining TIME-GCM curves illustrate comparable EIA peak densities for the IGRF simulations with and without tropospheric tidal forcing. They provide further evidence that in-situ ionosphere-thermosphere coupling processes introduce EIA longitudinal variations; specifically, a 3-peaked structure at F-region altitudes. But, the TIME-GCM IGRF results confirm that the 4-peaked structure also seen in the IMAGE-FUV data can be attributed to the tropospheric tidal sources. The model EIA enhancement in the American sector (near 100°W) significantly underestimates the observed enhancement. Further, the observed peaks are shifted in longitude with respect to the TIME-GCM peaks. These shifts may be attributable to differences between the climatological GSWM tidal forcing for the month of March and the plausible evolution of tropospheric tides during the March–April 2002 period characterizing the observations. In spite of these differences in detail, the TIME-GCM IGRF results account for the FUV zonal variation that depends on the height-integrated 135.6-nm volume emission rate, which

is roughly proportional to the square of the peak electron density (i.e., NmF_2^2).

4. Discussion and Summary

[13] The GSWM forcing at the TIME-GCM lower boundary includes aggregate tidal perturbations associated with 13 zonal wavenumbers (i.e., westward propagating wavenumber 6 through eastward propagating wavenumber 6) for both diurnal and semidiurnal harmonics. However, only a subset of these waves propagates upward into the MLT, including the migrating components and the DE3 [Hagan and Forbes, 2002, 2003]. Hagan and Forbes [2002] noted that the DE3 dominates the GSWM diurnal temperature and zonal wind responses near 115 km during most of the year (i.e., except May, June, and August). Bispectral frequency-wavenumber analyses and associated Fourier fits to our TIME-GCM IGRF results confirm strong signatures of the migrating diurnal and semidiurnal tides in the MLT during March (not illustrated) and a dominant DE3 tide at E-region altitudes. Figure 4 illustrates the TIME-GCM DE3 zonal wind amplitude and phase as a function of latitude and altitude. The amplitude grows with increasing altitude, peaking at a value in excess of 50 m/s in the tropical lower thermosphere (i.e., ~ 115 km) and dissipating aloft (Figure 4). Although it undergoes significant dissipation above the peak, the wave continues to propagate well into the upper thermosphere, maintaining an amplitude of more than 10 m/s above 200 km over the equator. DE3 zonal wind phase contours largely exhibit the downward progression that characterizes an upward propagating wave and point to a vertical wavelength of the order of 60–70 km in the middle atmosphere. The DE3 is excited by tropical tropospheric latent heat release in the GSWM [Hagan and Forbes, 2002], so the IMAGE-FUV data and our TIME-GCM results provide corroborating evidence that deep convective cloud systems affect the Earth’s ionosphere in

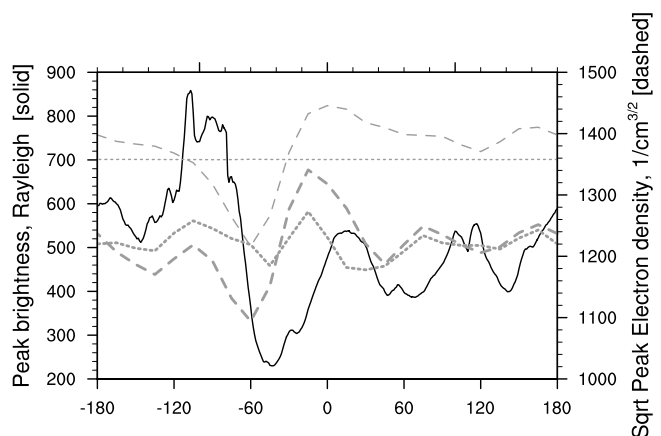


Figure 3. The square root of peak electron density at 2000 Solar Local Time between 0° and 45°N and 250 and 500 km versus longitude for the TIME-GCM standard model run with (thick long dash) and without tropospheric tides (thin long dash) and for the aligned dipole field with (thick dot) and without (thin dot) tropospheric tides along with IMAGE-FUV peak brightness measurements (solid) after Immel *et al.* [2006].

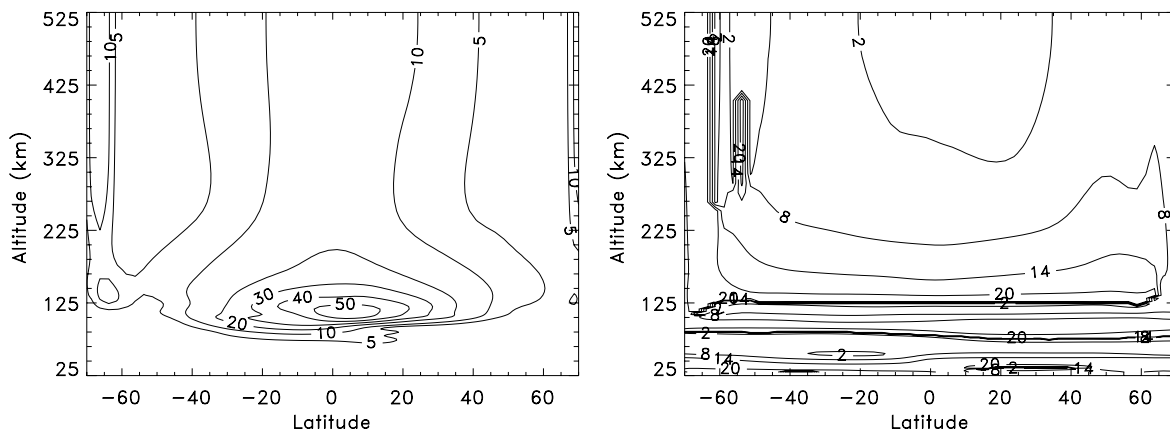


Figure 4. (left) Zonal wind amplitude (m/s) and (right) phase (local solar hours at 0° longitude) of the eastward propagating zonal wavenumber-3 diurnal tide versus latitude between 70°S and 70°N and altitude (km) from the TIME-GCM standard IGRF model run.

measurable ways, by modulating the E-region dynamo and affecting the F-region aloft. In a follow-on report we will explore the persistence of these DE3 effects during other local times, seasons, and solar cycle conditions, along with upper atmospheric impacts of other tidal components of the lower atmospheric origin.

[14] **Acknowledgments.** The authors thank B. Foster for his contributions to the development of the high-resolution version of the TIME-GCM and W. Wang and J. Forbes for comments on the initial draft of this report. The National Center for Atmospheric Research is supported by the National Science Foundation. IMAGE FUV analysis is supported by NASA through Southwest Research Institute subcontract 8382 to the University of California, Berkeley, under contract NAS5-96020.

References

- Appleton, E. V. (1946), Two anomalies in the ionosphere, *Nature*, *157*, 691–693.
- England, S. L., S. Maus, T. J. Immel, and S. B. Mende (2006a), Longitudinal variation of the E-region electric fields caused by atmospheric tides, *Geophys. Res. Lett.*, *33*, L21105, doi:10.1029/2006GL027465.
- England, S. L., T. J. Immel, E. Sagawa, S. B. Henderson, M. E. Hagan, S. B. Mende, H. U. Frey, C. M. Swenson, and L. J. Paxton (2006b), Effect of atmospheric tides on the morphology of the quiet time, postsunset equatorial ionospheric anomaly, *J. Geophys. Res.*, *111*, A10S19, doi:10.1029/2006JA011795.
- Evans, D. S. (1987), Global statistical patterns of auroral phenomena, in *Proceedings of the Symposium on Quantitative Modeling of Magnetospheric-Ionospheric Coupling Processes*, edited by Y. Kamide and R. A. Wolf, pp. 325–330, Kyoto Sangyo Univ., Kyoto, Japan.
- Fesen, C. G., G. Crowley, R. G. Roble, A. D. Richmond, and B. G. Fejer (2000), Simulation of the pre-reversal enhancement in the low latitude vertical ion drifts, *Geophys. Res. Lett.*, *27*, 1851–1854.
- Hagan, M. E., and J. M. Forbes (2002), Migrating and nonmigrating diurnal tides in the middle and upper atmosphere excited by tropospheric latent heat release, *J. Geophys. Res.*, *107*(D24), 4754, doi:10.1029/2001JD001236.
- Hagan, M. E., and J. M. Forbes (2003), Migrating and nonmigrating semi-diurnal tides in the upper atmosphere excited by tropospheric latent heat release, *J. Geophys. Res.*, *108*(A2), 1062, doi:10.1029/2002JA009466.
- Immel, T. J., E. Sagawa, S. L. England, S. B. Henderson, M. E. Hagan, S. B. Mende, H. U. Frey, C. M. Swenson, and L. J. Paxton (2006), Control of equatorial ionospheric morphology by atmospheric tides, *Geophys. Res. Lett.*, *33*, L15108, doi:10.1029/2006GL026161.
- Jadhav, G., M. Rajaram, and R. Rajaram (2002), A detailed study of equatorial electrojet phenomenon using Ørsted satellite observations, *J. Geophys. Res.*, *107*(A8), 1175, doi:10.1029/2001JA000183.
- Lin, C. H., W. Wang, M. E. Hagan, C. C. Hsiao, T. J. Immel, M. L. Hsu, J. Y. Liu, L. J. Paxton, T. W. Fang, and C. H. Liu (2007), Plausible effect of atmospheric tides on the equatorial ionosphere observed by the FORMOSAT-3/COSMIC: Three-dimensional electron density structures, *Geophys. Res. Lett.*, *34*, L11112, doi:10.1029/2007GL029265.
- Lindzen, R. S. (1981), Turbulence and stress owing to gravity wave and tidal breakdown, *J. Geophys. Res.*, *86*, 9707–9714.
- Lühr, H., S. Maus, and M. Rother (2004), Noon-time equatorial electrojet: Its spatial features as determined by the CHAMP satellite, *J. Geophys. Res.*, *109*, A01306, doi:10.1029/2002JA009656.
- Oberheide, J., Q. Wu, T. L. Killeen, M. E. Hagan, and R. G. Roble (2006), Diurnal nonmigrating tides from TIMED Doppler Interferometer wind data: Monthly climatologies and seasonal variations, *J. Geophys. Res.*, *111*, A10S03, doi:10.1029/2005JA011491.
- Roble, R. G. (1995), Energetics of the mesosphere and thermosphere, in *The Upper Mesosphere and Lower Thermosphere: A Review of Experiment and Theory*, *Geophys. Monogr. Ser.*, *87*, edited by R. M. Johnson and T. L. Killeen, pp. 1–21, AGU, Washington, D. C.
- Roble, R. G. (1996), The NCAR thermosphere-ionosphere-mesosphere-electrodynamics general circulation model (TIME-GCM), in *STEP Handbook on Ionospheric Models*, edited by R. W. Schunk, pp. 281–288, Utah State Univ., Logan.
- Roble, R. G., and E. C. Ridley (1994), A thermosphere-ionosphere-mesosphere-electrodynamics general circulation model (TIME-GCM): Equinox solar cycle minimum simulations (30–500 km), *Geophys. Res. Lett.*, *21*, 417–420.
- Sagawa, E., T. J. Immel, H. U. Frey, and S. B. Mende (2005), Longitudinal structure of the equatorial anomaly in the nighttime ionosphere observed by IMAGE/FUV, *J. Geophys. Res.*, *110*, A11302, doi:10.1029/2004JA010848.
- Vladimer, J. A., P. Jastrezebski, M. C. Lee, P. H. Doherty, D. T. Decker, and D. N. Anderson (1999), Longitude structure of ionospheric total electron content at low latitudes measured by the TOPEX/POSEIDON satellite, *Radio Sci.*, *34*, 1239–1260.
- S. L. England and T. J. Immel, Space Sciences Laboratory, University of California, Berkeley, Berkeley, CA 94720, USA.
- M. E. Hagan, A. Maute, A. D. Richmond, and R. G. Roble, High Altitude Observatory, National Center for Atmospheric Research, Boulder, CO 80307–3000, USA. (hagan@ncar.edu)